OPPORTUNITIES AND CHALLENGES TO USE POROUS MEDIA FOR EXHAUST GAS TREATMENT

Y. Yuan*, M. Vayasi[†], S. Staudacher*, G. Lamanna[†]

* Institut für Luftfahrtantriebe, Universität Stuttgart, Stuttgart, Germany

† Institut für Thermodynamik der Luft- und Raumfahrt, Universität Stuttgart, Stuttgart, Germany

Abstract

Aircraft, relying on fuels that release water vapour as part of the exhaust flow, may potentially generate contrail cirrus thereby altering the radiative forcing of climate. The use of ultra-high bypass engines makes exhaust gas treatment in the core flow conceivable, due to its overall low contribution to thrust generation. Successful implementation of this concept is largely determined by the possibility of recovering water and its precursors from the core flow, while minimizing the corresponding pressure losses and optimizing the integration of the required systems into the engine and aircraft structure. The use of porous media for condensation of water vapor could significantly enhance water recovery while simultaneously reducing soot emissions. The opportunities and challenges of using porous media in an ultra-high bypass ratio are discussed from three perspectives. First, the boundary conditions set by the thermodynamic engine cycle are discussed including the expected degrees of saturation and the relevant thermodynamic exchanges rates. It is these considerations that lead to a first process design and target system parameters. Second, the Schmidt-Appelman criterion is employed to estimate the percentage of water recovery from the core flow, required to significantly reduce the probability of producing persistent contrails. This step is mandatory in order to set appropriate requirements for the efficiency of the water removal concept and identify suitable forms of porous media (or alternatively functional condensation surfaces), their placement and operating conditions. The main parameters describing them and their relevance for the process design are also discussed. Third, a 1D approach to generally model porous media is presented. Whilst a generalized modelling approach is conceivable, it turns out that the underlying main parameters are highly dependent on the porous media chosen. Simple scaling rules allowing the description of the performance of different media have not been found. Consequently, choosing a particular porous media calls for ad hoc numerical and experimental efforts to provide the data required to assess its impact on the exhaust gas treatment in an ultra-high bypass ratio engine.

> Keywords Water Recovery, Contrail, Porous Media, Performance

1. INTRODUCTION

In recent years, there has been an increased interest in reducing the environmental footprint of aviation. In this work, we mainly concentrate on developing mitigating solutions to reduce the radiative forcing (RF) caused by air traffic. The term radiative forcing refers to a change in the Earth's radiation balance due to a perturbation of anthropogenic or natural origin, which causes an imbalance between solar incident radiation and the radiation emitted from the Earth's surface. The total aviation RF is caused by both CO2 and non-CO2 emissions. The non-CO2 emissions encompass nitrogen oxides (NOx), aerosols and their precursors (soot and sulphate) and water vapour. The last three components directly contribute to the formation of aircraft-induced clouds (AIC), which mainly consist of persistent contrails and contrail cirrus. In literature, the actual aviation RF is controversially discussed. According to Lee et al. [1], it amounts to roughly 3-5% of the total anthropogenic forcing. These estimations were based upon the predictions from simplified climate models and by extrapolating empirical correlations [1]. Similarly, Kärcher [2] evaluated the aviation RF as a percentage of the total radiative forcing caused by human activities in 2011. He found it to be of the order of 4% relative to pre-industrial times. Within this percentage, aircraftinduced clouds (AIC) deliver the predominant contribution (roughly 55%) to the total aviation-induced RF [2]. In absolute terms, this amounts to 50 (20-150) mW m^{-2} . The correlation between AIC and positive RF has been questioned by several authors [3–6] on the basis of satellite data and more advanced climate models. A comprehensive, divulgative review was presented by Myhre et al. [5], which places emphasis on the complex interplay among natural/anthropogenic aerosols, cloud formation and global climate. The complexity is due to the fact that aerosols may cause a large range of possible climate effects, depending upon their composition, size, number density and induced changes in the microphysical properties of cirrus clouds [6]. The current lack of understanding of this interplay limits our knowledge of climate change and results in high uncertainties in its predictions [5, 6].

Hereafter, a brief summary of the current state-of-the-art is presented with a strong focus on aviation-generated aerosols. The latter are produced in the atmosphere by condensation of water vapour on precursors particles, typically sulfate and nitrate emitted from fossil fuel combustion. This occurs when the exhaust gas mixes with the low temperature atmosphere, typically at cruise altitudes of about 33000 ft - 42000 ft. As the plume cools down, a level of high supersaturation over liquid water can be locally achieved due to the simultaneous decrease of the H2O equilibrium vapour pressure. This triggers the heterogeneous condensation process and the formation of contrails. For dry or subsaturated air, contrails are short-lived (0.1-10 min) and rapidly evaporate, as the plume becomes more dilute by entraining ambient dry air.

Short-lived contrails are line-shaped and have no impact on the RF [2]. Instead, if turbulent mixing occurs in cold, moist air, then the plume aerosols grow into water droplets that eventually freeze and form ice crystals by uptake of water vapour. This process eventually leads to the formation of persistent contrails, as described by Kärcher [2]. The further evolution of the ice crystals largely depends upon fluid-dynamical processes in the downstream wake region (vortex regime). When ice-supersaturated ambient water vapour is entrained, the ice crystals will ultimately sublimate. The transition into contrail cirrus is mainly controlled by meteorological factors (e.g., wind, humidity, cloud coverage) and microphysical local processes [4, 6], which at last determine the extension of ice cloud layers, their shape, depth and lifetime.

In this context, it is important to mention that both droplet and ice-particle growth are strongly influenced by the mixing of different aerosols of anthropogenic or natural origin. Moreover, they have a strong impact on the resulting RF of aerosols and more generally of aircraft-induced clouds (AIC). Indeed, as pointed out by Myhre et al. [3], it is necessary to distinguish between the direct aerosol effect and the cloud albedo effect. They both contribute to the total Earth's radiative forcing (RF) and their importance is directly connected to the aerosols' properties, location and interplay with cloud coverage. The direct aerosol effect refers to the amount of radiation directly scattered (or absorbed) by the aerosols. This contribution to the RF is less efficient, when scattering (absorbing) aerosol are located above a bright (dark) surface, because the solar radiation is reflected (absorbed) anyway. The opposite occurs when absorbing aerosols are positioned above clouds, which are the main contributors to the total reflection of solar radiation back to space. The cloud albedo effect refers to the enhanced reflection and cooling of a cloud when aerosols act as cloud condensation nuclei (CCN) or ice nuclei (IN). Consequently, for a more realistic estimation of the total aviation RF, it is necessary to consider a global probability density function (PDF), which includes not only the effect of the individual aerosol components, but also the interplay between synoptic meteorological factors and aerosol-cloud microphysics [3]. The macroscopic result is that the most probable value for the total RF, accounting for both the direct aerosol effect and the cloud albedo effect, is $-1.2~\mathrm{Wm^{-2}}$, which implies cooling instead of heating the Earth's atmosphere. This finding was recently corroborated by the predictions of Beer et al. [6]. The authors focused only on the effect of ice-nucleating particle on the Earth's RF by using a global aerosol-climate model. They found a negative RF, in the range of -28 till -55 mWm² due to uncertainties in the freezing properties of ice-nucleating particles. This estimation could increase by one order of magnitude (-42 to -340 mWm²) in presence of updraught speeds. On the other side, the numerical results also indicated that overseeding the cirrus clouds could often lead to a positive RF (up to 86 mWm²) depending upon the number density of seeded ice-nuclei. These findings pave the way towards the development of engineered solutions, where ice-nucleating particles are used efficiently for seeding cirrus clouds as a means to reduce global warming.

The preceding discussion has shown the importance of developing novel technologies that enable a controlled release of water vapour and its precursors in the exhaust flow, as a means to mitigate or even positively exploit the environmental footprint of aviation. This paper presents the

first steps towards the evaluation of novel concepts and is organised as follows. First, we present a brief overview of the available technologies for water recovery. Second, the Appleman [7] and Schumann [8] criterion is used to assess how the water content in the engine exhaust should be influenced in such a way to mitigate the formation of AIC. Third, as alternative to the use of heat exchangers [7], we investigate the possibility of using a porous medium for water and soot recovery from the exhaust gas. For this purpose, a 1D numerical model has been developed to provide a first assessment of this technology at system level.

2. AVAILABLE TECHNOLOGIES

Reducing the vapour amount of the jet engine exhaust is challenging because the exhaust gas features stagnation temperatures in the range of 600 to 800 K and a water vapor mass content of about 3%. These operating conditions pose strict requirements from a thermodynamic and operational point of view. From a thermodynamic standpoint, it is necessary to cool down the exhaust gas to very low temperatures to enable the condensation of water vapour. On the other hand, in order not to strongly penalise the engine's efficiency in producing its design level of thrust, it is also necessary to raise the exhaust gas temperatures again after water recovery. It is therefore self-evidents that the availability of efficient heat exchangers represents the first bottleneck for water recovery technologies. The second bottleneck is represented by the need to design suitable structures and surfaces for capturing and removing the condensed water. A brief review of the available technologies is presented hereafter.

Utriainen and Sunden [9] discussed different types of heat exchangers, which could be potentially used in gas turbines to remove heat from the exhaust gas. In addition, heat recovery from the engine exhaust using existing heat exchanger technologies was successfully demonstrated in the European Research Project Clean [10–12]. The Intercooled Recuperated Aero-Engine Concept (IRA) [13] expanded the use of heat exchangers in jet engines from removing heat from the exhaust gas to intercooling the air leaving the low pressure (LP) compressor with cold bypass air, before it enters high pressure compressor [13]. As a consequence of the application of these two heat exchangers, the fuel consumption of the engine is decreased with the overall pressure ratio (OPR) being limited due to the boundary conditions introduced by the exhaust gas heat recovery. Both of these factors positively influence the NOX and CO2 emission. Nevertheless, intercooler and recuperator, together with the supporting pipes and ducts, negatively impact the total engine weight. A comprehensive comparative evaluation of different technical solution for future aircraft gas turbines showed that compressor intercooling, exhaust gas heat recovery and pressure rise combustion are promising technologies for future jet engines [14]. Yet, there is an ongoing discussion on the application of heat exchanger technologies in jet engines concerning their impact on the weight and overall engine efficiency (see e.g. [15]).

Steam Injecting and Recovering Aero-engine Concept (SIRA) [16], also termed Water-Enhanced Turbofan Concept (WET), is based on water injection before combustion, its condensation and recovery after the turbine section. This concept promises a significant reduction of the NOX emissions thanks to wet combustion, a certain improvement in engine efficiency as well as a reduction of

CC BY 4.0

particle emissions and hence in contrail formation. Yet, the components required for condensing, recollecting and evaporating the water negatively impact the engine weight and size. Finally, we point out that concepts for water recovery from the hot engine exhaust have not been studied for current turbofan engine architectures. In this context and with the aim to decrease its potential negative impact on aircraft and engine performance, porous media with high porosity are considered. They represent potentially good candidates because of their low total density and large surface area, which allows to enhance simultaneously heat transfer and condensation rate. Apart from water recovery, porous media also offer interesting potentials for waste heat and soot recovery as well as noise reduction.

2.1. Porous Media

This section introduces the main parameters and requirements, needed to study the interaction between exhaust gas and porous media (pm) at system level. For this purpose, macroscopic properties of porous media, such as porosity, permeability and heat transfer coefficient, have to be specified. The latter not only reflect the main characteristics of porous media at the macroscopic scale, but also significantly influence its performance as water removal unit. Examples of porous media with different porosity are visualized in Fig. 1.



FIG 1. Porous media with different porosity

The porosity ε is defined in Eq. 1 as the ratio of the void volume V_f to its total volume V_{total} . It is an important factor to determine the thermal performance and transport capability of porous materials [17]:

(1)
$$\varepsilon = \frac{V_f}{V_{total}}$$

The tortuosity τ is defined in Eq. 2. It describes the complex structure of the media and its impact on transport properties. It is defined as the ratio of the path length traversed by the fluid, L_f to the sample length, L [18]:

(2)
$$\tau = \frac{L_f}{L}$$

As a general rule of thumb, large tortuosity results in larger viscous drag force and enhanced heat transfer during fluid transport within the pm tortuous structures. The permeability k is defined in Eq. 3:

(3)
$$k = \frac{v\mu\Delta x}{\Delta P}$$

Here, v is the fluid velocity, μ is the dynamic viscosity, Δx is the thickness of the porous media and ΔP is the pressure

difference applied. The permeability provides a measure for the pressure loss of the fluid resulting from the blockage effect of the solid structure in the porous media. It was first introduced by Darcy, who assumed a linear dependence between shear forces and pressure loss. Its definition was later expanded by Forchheimer, who assumed a quadratic dependence to include the effect of inertial forces [17]. The convective heat transfer coefficient h characterizes the heat transfer within the porous media. Similarly, the interfacial heat transfer coefficient h_{amb} characterizes the average heat transfer between the outer surface of porous media and the ambient. Values of these two coefficients are de-

pendent on fluid velocity, the inner structure and material

2.2. Definition of Test Case and Requirements

properties of porous media [17, 19].

The usage of porous media for heat transfer and water recovery is discussed using an ultra-high bypass ratio engine as an example. It features a bypass ratio of 17 at cruise conditions. The nozzle configuration embraces separate nozzles for core and bypass flow. This is deemed to be a favourable case, since the contribution of the core flow to the engine thrust is relatively low. Note that the water recovery unit is assumed to be placed in the core exhaust flow.

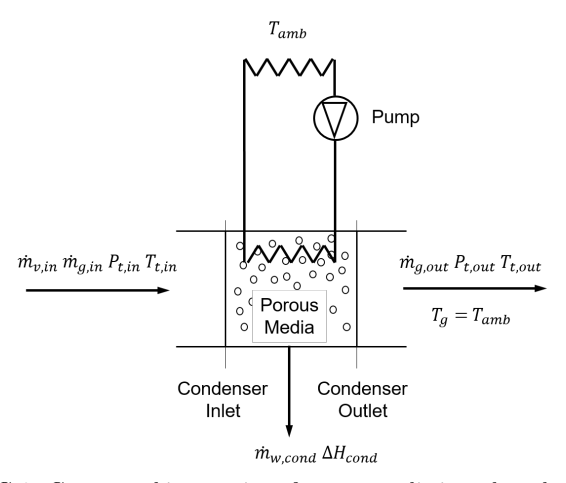


FIG 2. Conceptual integration of porous media into the exhaust flow $\,$

This integration is conceptually depicted in Fig. 2. As a first step, it is assumed that cooling and water separation both are taking place in a section of the annulus containing the porous media, even though the associated pressure and temperature drop will negatively impact the engine efficiency. The bypass air flow or the ambient environment are potential heat sinks for the cooling circle. A pump is employed to remove the condensed water continuously. The assumed boundary conditions for the water recovery unit are listed in Tab. 1.

Parameters	Value	Unit
Vapour mass fraction	0.035	-
Gas velocity	241.847	m/s
Gas static temperature	595	K
Gas static pressure	30.6461	kPa
Ambient temperature	275	K

TAB 1. Engine cycle parameters [20, 21]

The performance requirements of the water recovery unit are derived using the Schmidt-Appleman mixing model. The latter basically describes the mixing of exhaust gas with the ambient air by employing a linear 1D model. The slope of the mixing line is defined by several parameters, such as the plume pressure (P), the specific heat of combustion (Q), the emission index of water (EI_{H_2O}) and the propulsion efficiency of the engine(η)

(4)
$$G = \frac{EI_{H_2O}C_pP}{\varepsilon Q(1-\eta)}$$

where ε denotes the molar mass ratio between water and air and C_p the isobaric specific heat capacity of air. The selected values for the above parameters are reported in Tab. 2, assuming the use of kerosene as fuel.

Parameters	Value	Unit
Specific combustion heat Q	43	$ m MJ~kg^{-1}$
Water emission index EI_{H_2O}	1.25	${\rm kg~kg^{-1}}$
Isobaric specific heat capacity of air C_p	1004	$\begin{array}{c} \rm J~kg^{-1}\\ \rm K^{-1} \end{array}$
Overal efficiency η	0.386	-
Molar mass ratio $\varepsilon = \frac{M_{water}}{M_{air}}$	0.622	-
Gas Constant of water R_w	461.5	${ m J~kg^{-1}} \ { m K^{-1}}$
Gas Constant of air R_a	287.05	$\begin{array}{c} \rm J~kg^{-1} \\ \rm K^{-1} \end{array}$

TAB 2. Engine parameters for kerosene as fuel required to calculate slope G

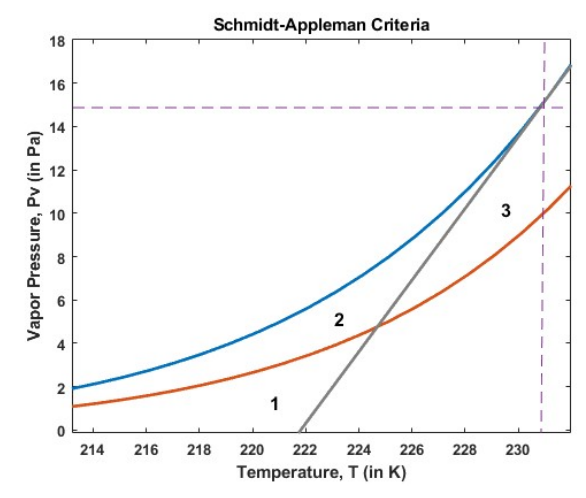
The overall efficiency of the engine η is defined as

(5)
$$\eta = \frac{F V}{Q \dot{m_f}}$$

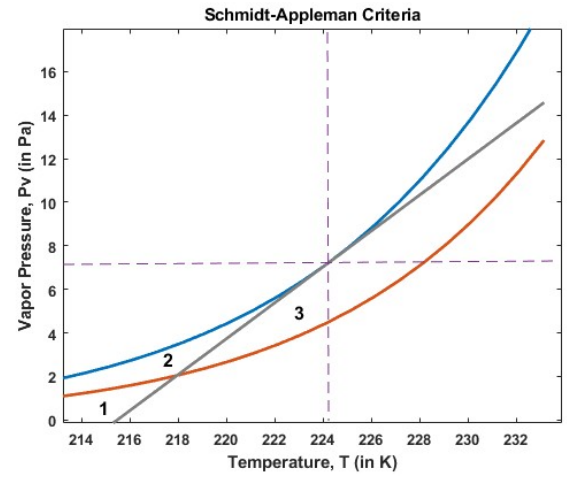
with F denoting the thrust, $\dot{m_f}$ represents the fuel mass flow rate and V the air speed. The overall propulsion efficiency in Tab. 2 results from the ultra-high by-pass ratio design of the engine [20]. Fig. 3a shows the liquid (blue) and ice (red) saturation lines, together with the mixing (black) line with slope G. The latter describes the possible mixing states between the gas exhaust and the ambient air, as derived from the linear 1D model of Schmidt-Appelman. With higher engine efficiency, the slope of mixing line increases and results in high threshold temperature for contrail formation, represented by the point of tangency between the liquid saturation curve (blue line) and the mixing line. In this context, it is necessary to introduce the concept of supersaturation S, defined in Eq. 6 as the ratio between the vapour partial pressure (P_v) and the saturation (equilibrium) pressure (P_s) at a given temperature

(6)
$$S = \frac{P_v}{P_s}$$

For condensation to occur, the following requirement must be satisfies $S \geq 1$. The peculiarity of the SA criterion is that they set S=1 as the onset for contrail formation, which provides a conservative estimate for the occurrence of contrails. As shown in Fig. 3a, the Schmidt-Appleman graph can be divided into three regions, namely 1, 2 and 3 according to the classification proposed by Wolf and Bellouin [22]. In region 1, the mixture of exhaust gas and air is undersaturated with respect to ice. In this case, the nonpersistent, short-lived contrails are formed, as the engine plume does not reach the required saturation level for the



(a) $EI_{H_2O} = 1.25$, When no water is removed



(b) $EI_{H_2O} = 0.625$, When 50% water is removed

FIG 3. Schmidt-Appleman Criteria for different EI_{H_2O}

onset of condensation. In region 2, the mixing state within the plume is supersaturated with respect to ice. As a result, persistent contrails can be formed when ice-supersaturated conditions are present in the atmosphere. Region 3 represents a potential reservoir, where already formed contrails can spread depending on synoptic meteorological factors and updraught velocities. This region is not considered further in this work. In the following, the Schmidt-Appelman mixing model is employed to estimate the percentage of water recovery from the core flow, required to significantly reduce the probability of producing persistent contrails. The result of this exercise is shown in Fig. 3b by lowering the water emission index EI_{H_2O} by 50%, specifically from 1.25 (in Fig. 3a) to 0.625 (in Fig. 3b). As can be seen, both the onset temperature for condensation and the extension of region 2 are significantly reduced, thus considerably mitigating the formation of persistent contrails. This also implies a target of at least 50% water recovery for the porous media technology. To better highlight the implications of water recovery on the development of the plumes, Fig. 4 shows the variation in saturation ratio as the gas exhaust mixes with ambient air for different values of the water emission index (EI_{H_2O}) . Assuming the same level of ambient relative humidity with respect to liquid water and ice (i.e. $S_{ice} = S_{water}$), it also shows that the local supersaturation with respect to ice is always higher compared to that of water. The plume supersaturation is

calculated using the model proposed by Jensen et al. [23], yielding

(7)
$$S_{w,plume} = \frac{n_{w,amb}}{n_{sat,i}(T_{pl})} + \frac{n_{air}C_pEI_{H_2O}\Delta TR_w}{n_{sat,i}(T_{pl})Q(1-\eta)R_d}$$

In this equation, the local supersaturation ratio in the plume can be calculated with regards to the vapor pressure equilibrium (saturation) curves for ice and liquid water, respectively. where $n_{w,amb}$ and $n_{sat,i}$ are the number density of ambient water vapor and number density of saturated water vapor respectively, n_{air} is the number density of air, R_d and R_w are the gas constant of dry air and water vapor. ΔT is the difference in plume temperature (T_{pl}) and ambient temperature (T_{amb}) . Figure 4 corroborates the previous statement. As the plume cools down by mixing with the cold ambient air, the local level of supersaturation can be drastically reduced by decreasing the water emission index EI_{H_2O} , thus quenching the probability to generate persistent contrail formation. This provides an important requirement for the following discussion of the water recovery unit.

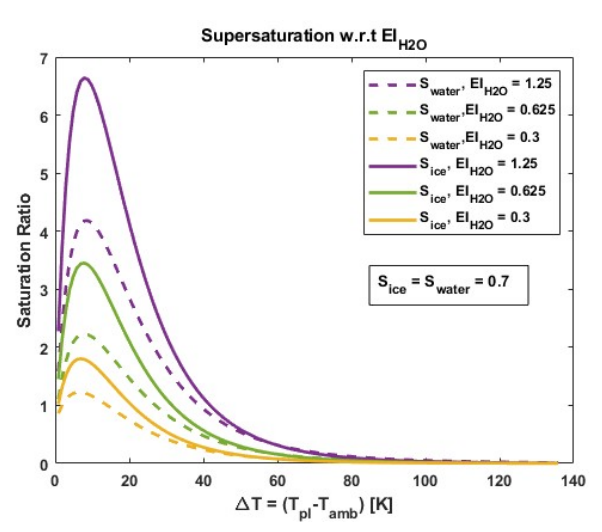


FIG 4. Local variation of the supersaturation ratio in the plume for different EI_{H_2O} values

3. PERFORMANCE ESTIMATION OF THE WATER RECOVERY UNIT

The water recovery unit equipping porous media is located after engine low pressure turbine (LPT) as demonstrated in Fig. 2. The hot moist exhaust gas at the inlet of this unit is with static temperature at the range of 500 to 600 K based on the cycle data of SynTrac engine [20]. It has to be considered, that the water recovery unit will be operated at different flight conditions and engine operating points. The question arises how to describe its performance over such a wide range of operating conditions. In a simplified approach, it is assumed that the exhaust gas needs to be cooled down below the dew point to realize condensation. In order to achieve this purpose, cold bypass gas is supposed to be utilized to keep the porous media's temperature at about 275 K. When the hot exhaust comes in contact with porous media's super-cooled surface, water vapor condensates. The liquid water generated during this process is supposed to be transported away instantly by a pump. The 1D approach which is used to model the involved physical processes in the porous media is described next.

3.1. Main Physical Processes and Assumptions in Condenser Modelling

As shown in Fig. 5, the physical processes appearing in porous media as condenser can be divided into three main categories as transportation of gas and liquid, heat transfer between different phases and condensation triggered by a suitable temperature.

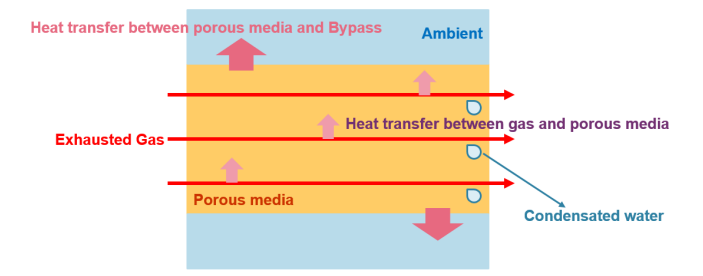


FIG 5. Physical processes in porous media

In this case of employing a porous media as condenser in an engine, hot moist gas is initially exhausted by the LPT and then passes through the porous media. During this transportation process, the gas temperature drops because of the heat exchange between it and porous material. When the gas temperature reaches the dew point, condensation is triggered and liquid water is removed for further usage. In order to derive performance maps which cover a wide range of operating points, these extremely complex processes in porous media are highly simplified with several assumptions. Therefore, the underlying equations reflecting necessary physical conservation are sufficient to derive the shape of the maps. Further detailed and accurate simulation of these processes are out of this article's scope. These applied assumptions and simplification are stated below.

- The heat transfer enhancement because of tortuosity in porous media structure during gas transportation is neglected considering the large void in porous media with high porosity.
- The heat conductivity in solid phase of porous media is overlooked as a consequence of its relative small value comparing with the huge amount of latent heat released and absorbed by porous media during condensation.
- Condensed water is regarded to be extracted from the condenser as soon as it is generated, so all the non-equilibrium effects relevant to this process are neglected.
- Similar to the Schmidt-Appleman model, condensation is regarded as a thermal-equilibrium process in this approach and is assessed with Mollier diagram. As a consequence, the water amount is overestimated in this 1D approach.

3.2. Fundamental Equations of 1D Model

All equations used in the 1D model are formulated based on conservation laws of moist exhaust gas and solid porous media structure, and further averaged by the corresponding volume for each phase. The fluctuation terms representing the tortuosity effects are neglected during this volume-average process, which in reality should be taken into account in Eq. 8 to 11. The detailed description of there equations are as follows.

(8)
$$\frac{d(\rho_g u_g)}{dx} = -\dot{m}_{w,cond}$$

Parameters	Value	Unit
Porosity ε	90%	-
Darcy's permeability k_{Da}	8×10^{-3}	m
Forchheimer's permeability k_F	6×10^{-1}	m^2
Heat transfer coefficient h_v	6×10^6	$\frac{W}{m^3K}$
Heat transfer coefficient $h_{s,amb}$	3.6×10^{5}	$\frac{W}{m^2K}$

TAB 3. Parameters of porous media

(9)
$$\frac{d(\rho_g u_g u_g)}{dx} = -\frac{dP_g}{dx} - \frac{\mu_g}{k_{Da}} u_g - \frac{1}{k_F} \rho_g u_g^2 - \dot{m}_{w,cond} u_g$$

(10)
$$\frac{d(\rho_g u_g(c_{v,g}T_g + \frac{1}{2}u_g^2))}{dx} = -\frac{d(P_g u_g)}{dx} - \frac{\dot{m}_{w,cond}c_{p,v}T_{t,g} + \frac{h_v}{\varepsilon}(T_s - T_g)}{\varepsilon}$$

(11)
$$\frac{h_v}{1-\varepsilon}(T_g - T_s) + \frac{\varepsilon}{1-\varepsilon} \alpha \dot{m}_{w,cond} \Delta H_{cond} = \frac{h_{s,amb}}{1-\varepsilon} (T_s - T_{amb})$$

Mass conservation Eq. 8 describes how moist gas mass changes during condensation in porous media. Mass loss of the gas is at the same amount of condensed water whose phase changes from gaseous into liquid. Its value is assessed by the Mollier diagram in this approach by assuming the condensed water amount as the decrease of the dry air's maximal ability in carrying vapour as the gas temperature is reducing.

Momentum conservation Eq. 9 reflects how gas pressure changes in porous media. This change is described by the two terms respectively with the Darcy permeability k_{Da} and the Fochheimer permeability k_F . The secondary pressure loss resulting from loss of vapour during condensation is described by the term with condensed water mass $\dot{m}_{w,cond}$ which also appears in Eq. 8.

Furthermore, Eq. 10 and 11 describe the energy conservation for the gaseous and the solid phase respectively. The heat exchange between these two phases are mirrored by the similar terms in both equations, which are also scaled by ε or $1-\varepsilon$. These two scaling factors represent different volume occupied by both phases accordingly. The heat transfer coefficient $h_{s,amb}$ and h_v in these terms reflect the ability of solid phase and gaseous phase to transfer heat to other contacting colder phases. Moreover, coefficient α in Eq. 11 describes that only certain fraction of latent heat ΔH_{cond} released by phase transition is transferred into solid porous media structure, while the rest remains in condensed water and is exported out of the condenser. In order to calculate these equations with numerical methods, the whole condenser is regarded as an ensemble of numerous elements. Each element serves as an elementary calculation cell and the whole model can be therefore solved with application of the Finite Difference Method. During the calculation, the value of properties from porous media are selected as shown in Tab. 3.

3.2.1. Dimensional Analysis of Porous Media as Con-

Under the purpose of revealing physical relationship between the change of different gas property parameters in

$\frac{T_{t,in} - T_{t,out}}{T_{t,in}}$	Total Temperature Loss Ratio
$\frac{P_{t,in} - P_{t,out}}{P_{t,in}}$	Total Pressure Loss Ratio
$rac{\dot{m}_{w,cond}}{\dot{m}_{v,in}}$	Condensation Rate
$\frac{k_{Da}}{D^2}, \frac{k_F}{D}$	Darcy Number
$rac{L}{D}$	Size of Porous Media
$\frac{h_{sf}D^2}{k_g}$	Nusselt Number
$\frac{h_{s,amb}D^2}{k_s}$	Biot Number
$rac{\mu_g c_{p,g}}{k_g}$	Prandtl Number
$rac{k_s}{k_g}$	Ratio of Thermal Conductivity
$\frac{\dot{m}_{g,in}}{k_g D}$	Péclet Number
$\frac{\Delta H_{cond}}{T_{g,in}c_{p,g}}$	Energy Ratio
$rac{\dot{m}_{g,in}}{D\mu_g}$	Reynolds Number
$rac{\dot{m}_{v,in}}{\dot{m}_{g,in}}$	Vapour Mass Fraction
-g,in	Temperature Ratio
TAB 4	1. Dimensionless Parameters

porous media in a general way, dimensional analysis is applied independently from the 1D modeling approach stated before. Firstly, the most relevant parameters of the processes in porous media are identified. They are parameters representing gas condition at condenser inlet, porous media characteristics and gas properties at condenser outlet together with condensed water amount. As a next step, dimensional analysis with Buckingham Pi theorem is applied and its results are shown in Tab. 4. The dimensionless parameters such as Nusselt number, Biot number, Prandtl number and Péclet number are neglected in the following analysis as a consequence of the simplifications mentioned before. Meanwhile, results from the 1D modeling approach are applied to calculate the value of the rest dimensionless parameters and enable the performance map generation conducted in the following section. As a similarity, the term containing latent heat ΔH_{cond} is also neglected, since latent heat only varies very slightly during the whole processes in porous media. Finally, a conclusion based on this analysis process can be drawn as follows: The condensation rate, the change of total temperature and total pressure from condenser's inlet to the outlet can be regarded as a functions of Reynolds number, inlet vapour mass fraction and temperature difference between the heat sink T_{amb} and the exhausted gas $T_{g,in}$. This conclusion builds up the foundation for generating performance map in the following sections.

CC BY 4.0

3.2.2. Performance Map

Based on the dimensional analysis above, the condenser performance is expressed using the relations which are summarized in Eq. 12.

(12)
$$\frac{T_{t,in} - T_{t,out}}{T_{t,in}}, \frac{\dot{m}_{w,cond}}{\dot{m}_{v,in}}, \frac{P_{t,in} - P_{t,out}}{P_{t,in}} = f(\frac{\dot{m}_{g,in}}{D\mu_g}, \frac{\dot{m}_{v,in}}{\dot{m}_{g,in}}, \frac{T_{amb} - T_{g,in}}{T_{g,in}})$$

Firstly, Fig. 6, 7 and 8 illustrate the condenser performance assuming a fixed vapour mass fraction of 3.5%.

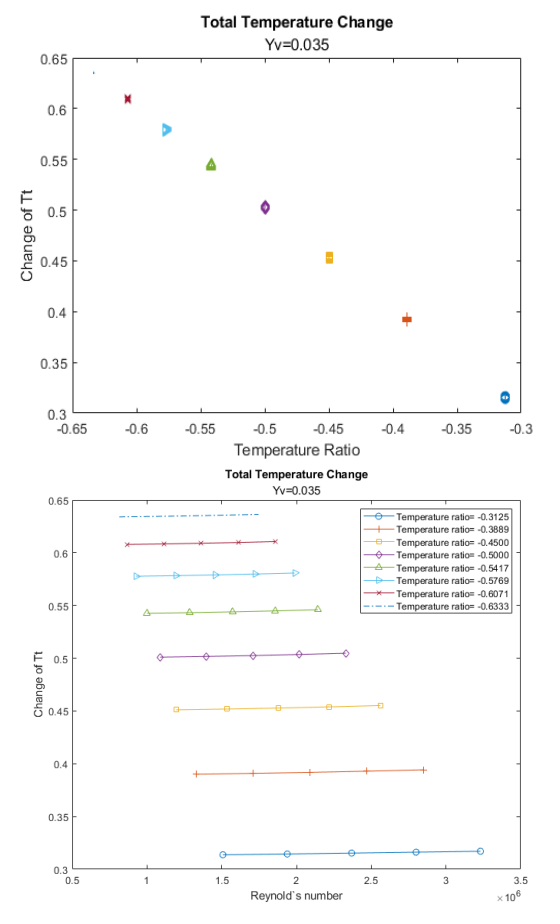


FIG 6. Change of Total Temperature

The upper plot in Fig. 6 shows that, with increasing temperature difference between exhaust gas and system sinker, the consequent heat transfer also increases and leads to higher gas total temperature decrease. However, influence from Reynolds number to this process as demonstrated in lower plot is not obvious. This deflection to the reality can be explained by the neglect of both heat conduction in solid phase and enhanced heat transfer resulting from structure tortuosity. These two facts together with increasing Reynolds number can actually lead to further increase in heat transfer. For example, it has been found that Nusselt number is a function of Reynolds number and Prandtl number [24]. As a consequence, the heat transfer modelled with this 1D approach is actually underestimated.

Fig. 7 demonstrates the relationship between condensation ratio and temperature difference or Reynolds number. Self-evidently in the upper plot, with increasing heat transfer, the level of condensation also becomes higher. Moreover, as illustrated in the lower plot, Reynolds number still plays

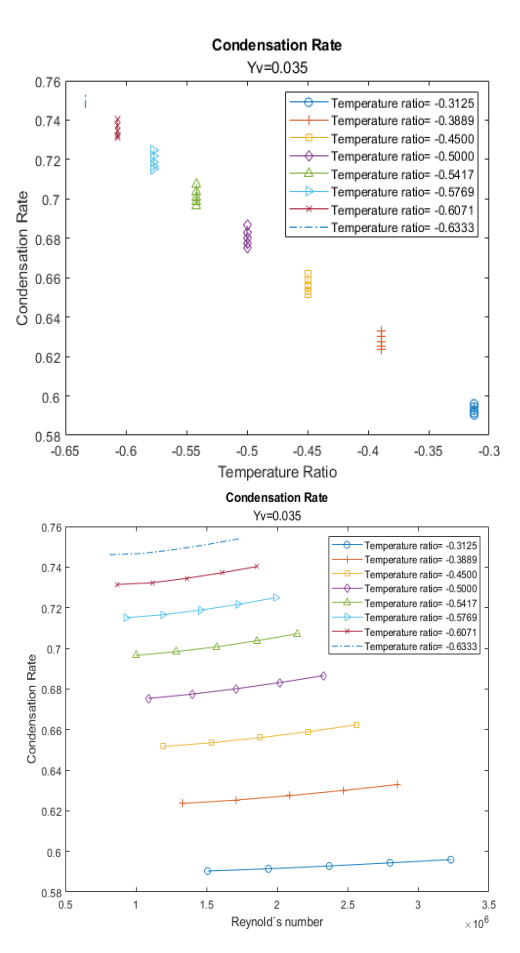


FIG 7. Change of Total Temperature

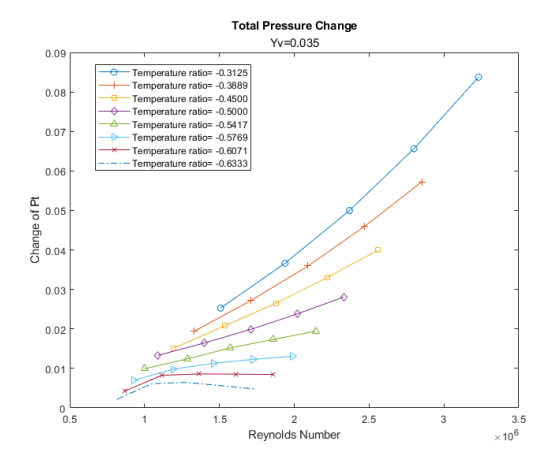


FIG 8. Change of Total Pressure

only a minor role in the change of condensation rate, considering high Reynolds number leads nearly no improvement in heat transfer.

Fig. 8 shows that with increasing Reynolds Numbers, the total pressure loss across the condenser can rise from about 2.527% to 8.374% for the case with largest temperature difference. This can be explained by tracing back to the Forchheimer and the Darcy term in the momentum conservation Eq. 9. In these two terms, pressure change is proportional to velocity or its square. As a consequence, higher velocity and hence higher Reynolds Numbers lead to high loss of total pressure.

However, it is also demonstrated in the same figure, with temperature difference between the heat sink and the

exhaust gas decreases from bottom curve to top curve, the slop of total pressure loss curve increases. This phenomenon is due to the fact that the increasing tendency of the pressure loss with increased Reynolds number could be compensated by enlarging the heat transfer between exhaust gas and system heat sinker. A similar phenomenon is also observed in the well-known Rayleigh line.

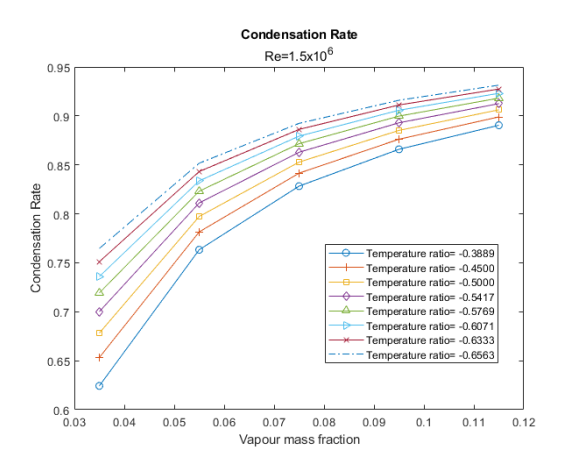


FIG 9. Condensation Rate

Next, Fig. 12, 9, 13 and 14 illustrate the condenser performance assuming a fixed Reynolds number of 1.5×10^6 . Several tendencies are observed.

As displayed in Fig. 9, the condensation rate increases with increasing vapour mass fraction and temperature difference, or in other words, the heat transfer level. These two increasing parameters can lead to changes of initial relative humidity, which is believed to be relevant to the condensation process [25]. Therefore, a closer look based on relative humidity is conducted with Fig. 10. It can be seen from this plot, for a constant temperature difference, a high initial relative humidity leads to a high condensation rate. The temperature difference itself on the other hand influences the level of this increase. For cases with high temperature difference, a slight increase of initial relative humidity leads to a large increase of condensation rate, while for other cases with lower temperature difference, the condensation rate rises only with obvious increase of relative humidity. Moreover, all the lines in Fig. 10 and Fig. 11 approach a limit of condensation rate of about 95%. This potential limit might indicate the existence of a maximal condensation rate in this condenser and further implies the existence of possible performance limit of this unit in decreasing contrail formation possibility.

Fig. 14 demonstrates that high condensation rate is also relevant for high pressure loss. This can be explained by the fact that with more vapour being condensed and extracted from condenser, the partial pressure of remaining vapour becomes less and finally a larger loss in total pressure of the whole moist gas mixture appears. Furthermore, this tendency is also related to the similar phenomenon shown in Fig. 12. With high vapour mass fraction, the total pressure loss is also huge. The key factor for this phenomenon is that, a high vapour mass fraction always results in a high condensation rate and therefore further indirectly leads to a high total pressure loss as demonstrated in Fig. 9.

Finally, as illustrated in Fig. 13, the opposite influences from temperature difference and condensation rate on total pressure loss does not leads to a kink point. This shows the

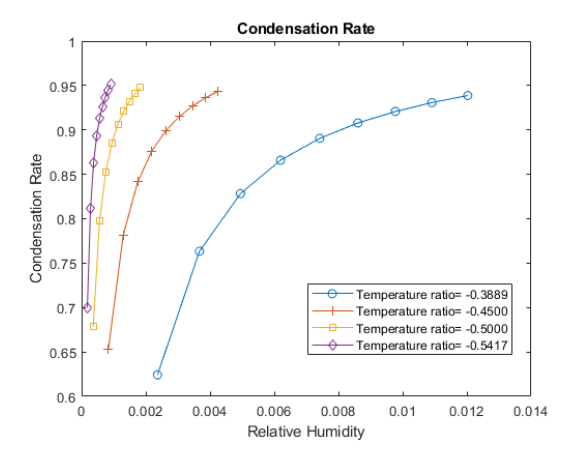


FIG 10. Condensation Rate with Relative Humidity

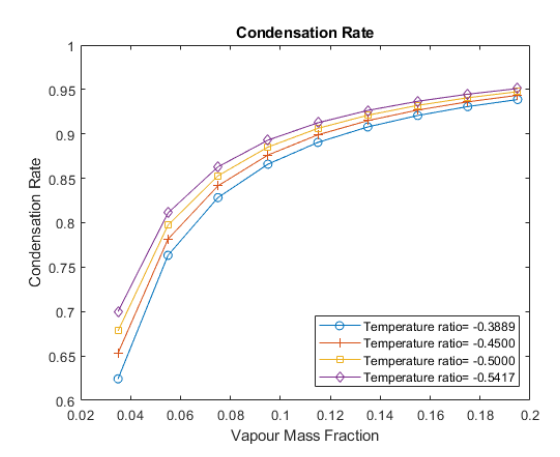


FIG 11. Condensation Rate with Vapour Mass Fraction

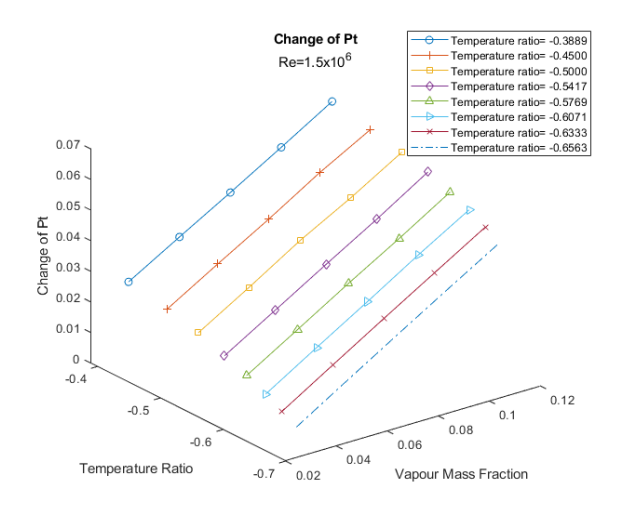


FIG 12. Change of Total Pressure

compensation effect by temperature difference overwhelms the negative effect from increased condensation ratio, and can be weakened by large condensation ratio as Fig. 14 shows.

Consequently several general tendencies are summarized. With high initial vapour fraction or relative humidity, high condensation efficiency could be realized by the condenser but with the price of high total pressure loss. On the contrary, with a high temperature difference between the heat sink and the exhaust gas, or in other words, with enhanced heat transfer, the condenser could still achieve a high con-

CC BY 4.0

Total Pressure Change with Condensation Yv=0.035, Re=1.5x10⁶

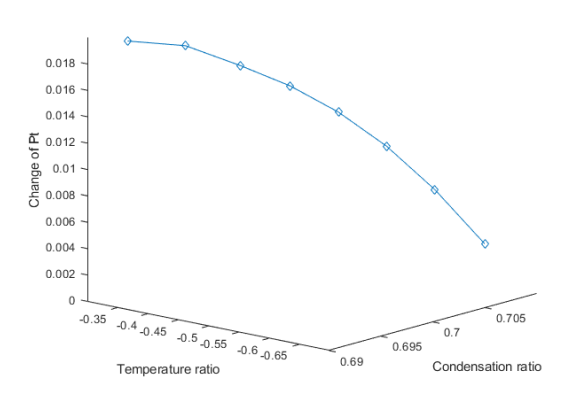


FIG 13. Pressure loss for fixed Re and Yv $\,$

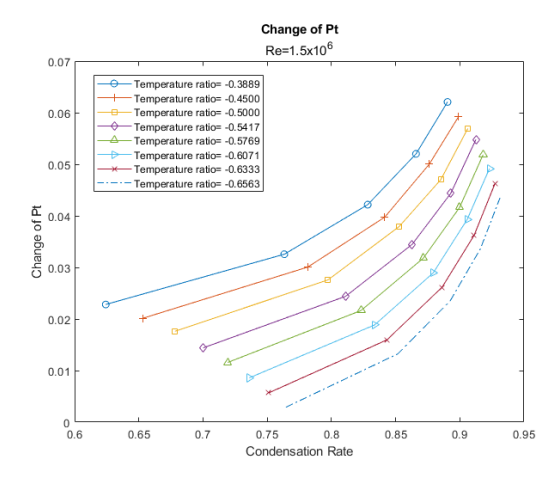


FIG 14. Pressure loss based on condensation and temperature change

densation rate with only relative small total pressure loss and the possibility to extract up to 95% of the vapour. Assuming the boundary conditions of the given used case and a porosity of 90%, the 1D Model indicates that the condenser could be able to extract about 64.82% of vapour from hot exhaust gas with a price of 2.67% total pressure loss. This fulfills the requirement of 50% exhaust gas vapour reduction derived from the Schmidt-Appleman approach.

From the perspective of engine performance, the mass of exhaust gas decreases with water extraction and its influence on the fuel consumption for generating same level thrust also awaits for further investigation. With the high losses, associated with the operation of the water recovery unit, the question arises, under which condition the operation of this equipment yields maximum benefit. The propose set of dimensionless parameters and the resulting performance maps of the porous media condenser provide a mean of answering this question based on mission simulations.

3.2.3. Challenges

Although porous media is a promising solution for eliminating contrails, waste heat removal and for noise reduction, there are a few challenges in using porous media.

• High temperature: Due to the high temperature of around 350°C in the core, it becomes difficult to condense the hot exhaust. The temperatures of the

- porous media should be maintained below the dew point temperatures for condensation to trigger.
- Less water concentration: The water vapor that is released from combustion accounts to only 3.5%. Therefore, the hot exhaust is under-saturated. Condensing low water concentration at high flow velocities using porous media is challenging. The small concentration of water vapor can get away along with the flow due to high velocities.
- Placement of Porous media: The main aim of the project is to remove at least 50% of the water coming out from combustion. For this porous media should be designed and placed in an intricate manner within the given space for effective results.

Contact address:

yiwen.yuan@ila.uni-stuttgart.de

REFERENCES

- [1] Lee D.S. et al. "Aviation and global climate change in the 21st century". In: Atmospheric Environment 43 (2009), pp. 3520–3537.
- [2] Kärcher B. "Formation and radiative forcing of contrail cirrus". In: Nature Communications 9 (2018), p. 1824.
- [3] G. Myhre. "Consistency Between Satellite-Derived and Modeled Estimates of the Direct Aerosol Effect". In: Science 325.5937 (2009), pp. 187–190.
- [4] Myhre G. et al. "Modelled radiative forcing of the direct aerosol effect with multi-observation evaluation". In: Atmospheric Chemistry and Physics 9.4 (2009), pp. 1365–1392.
- [5] G. Myhre et al. "Aerosols and their Relation to Global Climate and Climate Sensitivity". In: Nature Education Knowledge 4.5 (2013), p. 7. URL: https://www.nature.com/scitable/knowledge/ library/aerosols-and-their-relation-to-globalclimate-102215345/.
- [6] C. G. Beer, J. Hendricks, and M. Righi. "Impacts of ice-nucleating particles on cirrus clouds and radiation derived from global model simulations with MADE3 in EMAC". In: Atmospheric Chemistry and Physics 24.5 (2024), pp. 3217–3240.
- [7] Appleman H. "The formation of Exhaust Condensation Trails by Jet Aircraft". In: American Meteorological Society. Vol 34 (Jan. 1953).
- [8] Oberpfaffenhofen U. Schumann. "On conditions for Contrail formation from aircraft exhausts". In: Gebruder Borntraeger 0941-2948/96/0005-0004 (1996).
- [9] Utriainen E. and Sunden B. "Recuperators in Gas Turbine Systems". In: Turbo Expo: Power for Land, Sea, and Air Volume 3: Coal, Biomass and Alternative Fuels; Combustion and Fuels; Oil and Gas Applications; Cycle Innovations (June 1998).
- [10] Broichhausen K., Wilfert G., and Scheugenpflug H. "CLEAN the European Environmentally Friendly Engine Demonstrator". In: Proceedings of the 23rd International Congress OF Aeronautical Sciences. 2002-4.7.3 (Sept. 2002).

CC BY 4.0

- [11] Gerlach C. et al. "CLEAN Bench Adaption and Test for a Complex Demo Engine Concept at ILA Stuttgart". In: Procedings of the 17th International Symposium on Air Breathing Engines (ISABE), Munich.2005-1134 (Sept. 2005).
- [12] Wilfert G. et al. "CLEAN Validation of a GTF High Speed Turbine and Integration of Heat Exchanger Technology in an Environmental Friendly Engine". In: Proceedings of the 17th International Symposium on Air Breathing Engines (ISABE), Munich.2005-1156 (Sept. 2005).
- Boggia S. and Rüd K. "Intercooled Recuperated Gas Turbine Engine Concept". In: AIAA 4192 (2005).
- Schmidt F. "Vergleichende Bewertung der Arbeitsprozesse zukünftiger Fluggasturbinen". Institute of Aircraft Propulsion Systems, University of Stuttgart, Nov. 2020.
- Lundbladh A. and Sjunnesson A. "Heat Exchanger Weight and Efficiency Impact on Jet Engine Transport Applications". In: Procedings of the 16th International Symposium on Air Breathing Engines (IS-ABE), Cleveland Ohio. 2003-1122 (Sept. 2003).
- [16] Schmitz O., Klingels H., and Kufner P. "Aero Engine Concepts Beyond 2030: Part 1 - The Steam Injecting and Recovering Aero Engine". In: ASME 143.021001 (2021).
- Mayer B. "Investigations of Pressure Loss and Heat Transfer in a Regular Metallic Porous Structure". Institute of Aerospace Thermodynamics, University of Stuttgart, Jan. 2014.
- Graczyk K. and Matyka M. "Predicting porosity, permeability, and tortuosity of porous media from images by deep learning". In: Scientific Reports 21488 (2020).
- Teruel F. and Díaz L. "Calculation of the interfacial heat transfer coefficient in porous media employing numerical simulations". In: International Journal of Heat and Mass Transfer Volume 60 (2013).
- Iyer N.and Friedrichs J. "SynTrac B04 M1 Milestone Report". Institut für Flugantriebe und Strömungsmaschinen, Technische Universität Braunschweig, Feb. 2024.
- Yuan Y., Mehmood A., and Staudacher S. "Syn-Trac B04 M4 Milestone Report". Institut für Luftfahrtantriebe, University of Stuttgart, Mar. 2024.
- [22] K. Wolf, N. Bellouin, and O. Boucher. "Long-term upper-troposphere climatology of potential contrail occurrence over the Paris area derived from radiosonde observations". In: Atmospheric Chemistry and Physics (Preprint) (2022).
- Jensen E. "Environmental conditions required for contrail formation and persistence". In: Journal of Geophysical Research 103.D4 (1998), pp. 3929–3936.
- Kaviany M. Principles of Heat Transfer in Porous Media. 2nd ed. Springer Verlag.
- Böhrk L. "Implementation of a 1D model for droplet formation and growth to design a heat exchanger with phase change for the Water-Enhanced Turbofan (WET)". Institute of Aerospace Thermodynamics, University of Stuttgart, Apr. 2021.

NOMENCLATURE

Symbols	
ΔH_{cond}	Released Latent heat
\dot{m}	Mass flow
η	Propulsion efficiency of the engine
μ	Dynamic viscosity
ho	Density
au	Tortuosity
ε	Porosity
c_p	Isobaric gas heat capacity
c_v	Isochoric gas heat capacity
D	Condenser Diameter
EI_{H_2O}	Emission index of water
F	Thrust
G	Mixing Line/Slope
h	Heat transfer coefficient
h_{sf}	Interfacial heat transfer coefficient
k	Thermal conductivity
k_{Da}	Darcy's permeability
k_F	Forchheimer's permeability
L	Condenser Length
L_f	Path length traversed by the fluid
n	Number density
P	Static pressure
Q	Specific heat of Combustion
R	Gas constant
S	Supersaturation ratio
T	Static temperature
v, u	Velocity
V	Volume
V_f	Void volume of porous media

Subscripts

d	Dry air
g	Exhaust gas
s	Saturation (equilibrium) condition
s	Solid phase of porous media
v	Vapour
air	Air
amb	Ambient condition
cond	Condensed quantity
f	Fuel
in	Condenser inlet condition
i	Ice
out	Condenser outlet condition
plume	Plume condition
sat,i	Saturated water vapor
t	Total value
v	Vapour
w, amb	Ambient water vapor

Water